# Characterization of vacancy-type defects in Mg- and N-implanted GaN by using a monoenergetic positron beam

A. Uedono, R. Tanaka, S. Takashima, K. Ueno, M. Edo, K. Shima, S. F. Chichibu, J. Uzuhashi, T. Ohkubo, S. Ishibashi, K. Sierakowski, and M. Bockowski

***Abstract*—Annealing behaviors of vacancy-type defects in Mg and N-implanted GaN were studied by positron annihilation. The major defect species in as-implanted samples was identified as Ga-vacancy ($V_{Ga}$)-type defects. For Mg-implanted GaN with sequential N-implantation after annealing above 1000°C, the defect species were vacancy clusters such as $(V_{Ga}V_N)_3$. Due to the downward shift of the Fermi level position resulting from a partial activation of Mg, the charge states of defects tended to become positive. For N-implanted GaN, the size of the vacancy cluster started to decrease above 1200°C annealing, which was attributed to recombinations between $V_N$s coupled with $V_{Ga}$s and excess N atoms. The impact of sequential N-implantations on vacancies in Mg-implanted GaN was found to be most pronounced when the ratio of the concentration of N to that of Mg was three.**

***Index Terms*—GaN, ion implantation, vacancy defects, positrons**

## I. INTRODUCTION

Power devices are solid-state electronics that control and convert electrical energy. GaN is a key material for both present and future power electronics because of its excellent physical properties [1]. Currently, nearly all commercial GaN-based devices are fabricated using a lateral architecture. Due to the power-handling limitations of the lateral devices, however, vertical GaN power devices have garnered significant attention [2–4]. The fabrication of vertical devices requires a precisely controlled impurity doping technique, and this can be achieved using ion implantation. One of the obstacles to fabricating vertical devices has been the activation of an implanted p-type impurity: Mg. Recently, it was reported that ultra-high-pressure annealing (UHPA) is effective in obtaining a high activation rate of Mg implanted into GaN [4–6]. One of the reasons for the difficulties in activating implanted Mg is suggested to be the introduction of donor-like defects such as nitrogen vacancies ($V_N$s) [7]. Thus, the sequential implantation of N after Mg-implantation is also an effective technique to increase the Mg activation rate [4,8]. However, the reactions of defects and the formation of secondary defects during UHPA, as well as the impact of sequential N-implantation on them, are not well known. Positron annihilation spectroscopy is a useful technique for detecting vacancy-type defects in solids [9,10]. This technique has been used to study native and process-induced defects in GaN [11–15]. In the present study, we used a monoenergetic positron beam to study the annealing behaviors of vacancy-type defects in Mg- and N-implanted GaN. Photoluminescence (PL) measurements were carried out in order to correlate vacancy-type defects with non-radiative recombination centers (NRC). Secondary defects were characterized by low-angle annular dark-field scanning transmission electron microscopy (LAADF-STEM).

## II. EXPERIMENTAL

The present samples were undoped GaN grown on GaN substrates by metal-organic vapor phase deposition. Mg ions were implanted with energies ranging from 10 to 700 keV in order to obtain a 700-nm-deep box profile. The concentration of Mg ([Mg]) in the box profile was $1\times10^{18}$ cm$^{-3}$. After the Mg-implantation, N ions were implanted, and their depth profile was set to be similar to that of Mg. The concentrations of N in the box profiles were varied at $1\times10^{18}$, $3\times10^{18}$, and $1\times10^{19}$ cm$^{-3}$. After the implantation, the samples were annealed at temperatures up to 1450°C with an annealing time ($t_a$) of 5 minutes under a $N_2$ pressure ($P_{N2}$) of 1 GPa using a UHPA system [6]. UHPA with $P_{N2}$=0.5 GPa was also performed with $t_a$=5–60 min.

LAADF-STEM was used to examine the microstructure

This work was supported in part by the NEDO Program for Cross-Ministerial Strategic Innovation Promotion, the MEXT Program for Research and Development of Next-Generation Semiconductor to Realize Energy-Saving Society (JPJ005357), the MEXT Program for Creation of Innovative Core Technology for Power Electronics (JPJ009777), and JSPS KAKENHI (21H01826). This research was also partially supported by the Polish National Centre for Research and Development through project TECHMATSTRATEG-III/0003/2019-00 and Polish National Science Centre through project 2018/29/B/ST5/00338.

A. Uedono is with Institute of Pure and Applied Sciences, University of Tsukuba, Tsukuba, Ibaraki 305-8573, Japan (e-mail: uedono.akira.gb@u.tsukuba.ac.jp).

R. Tanaka, S. Takashima, K. Ueno, and M. Edo are with Advanced Technology Lab., Fuji Electric Co., Ltd., Hino, Tokyo 191-8502, Japan.

K. Shima and S. F. Chichibu are with Institute of Multidisciplinary Research for Advanced Materials, Tohoku University, Sendai 980-8577, Japan.

J. Uzuhashi and T. Ohkubo are with National Institute for Materials Science, Tsukuba 305-0047, Japan.

S. Ishibashi is with Center for Computational Sciences, University of Tsukuba, Tsukuba, Ibaraki 305-8577, Japan.

K. Sierakowski and M. Bockowski are with Institute of High Pressure Physics, Polish Academy of Sciences, Sokolowska 29/37, 01-142 Warsaw, Poland

Color versions of one or more of the figures in this article are available online at http://ieeexplore.ieee.org

using a Titan G2 80-200 (Thermo Fisher Scientific) microscope at an accelerating electron voltage of 200 kV. The samples were prepared using a focused-ion-beam (FIB) scanning electron microscope, the dual-beam Helios 5UX (Thermo Fisher Scientific). The sample thickness was 30 nm based on the intensity of backscattered electrons [16,17]. The depth distributions of Mg were measured by secondary ion mass spectrometry. PL spectra were measured at 13 K using a 325-nm He-Cd laser as an excitation source under a weak-excitation condition (38 $Wcm^{-2}$).

Vacancy-type defects in the samples were characterized using a monoenergetic positron beam. Details on this technique can be found elsewhere [9,10,12–14]. Doppler broadening spectra were measured using Ge detectors as a function of the incident positron energy ($E$), and they were characterized by the $S$ parameter. The spectra were also measured using a coincidence Doppler broadening technique [9]. The relationship between $S$ and $E$ was analyzed using the computer code VEPFIT [18]. The spectra were measured in darkness and under the illumination of a 325-nm He-Cd laser (Kinmon Koha, IR3802R-G). The Doppler broadening spectra were simulated by QMAS (Quantum MAterials Simulator) code [19] using the projector augmented-wave (PAW) method [20] and a plane-wave basis set. Details on applying QMAS to calculations of positron states and annihilation parameters in group-III nitrides are given elsewhere [21].

## III. Results and Discussion

Figure 1 shows the $S$ parameter of Mg-implanted GaN with sequential N-implantation ([N]=$1\times10^{18}$ $cm^{-3}$) before and after UHPA ($P_{N2}$=1 GPa) as a function of the incident positron energy $E$ [15]. The mean implantation depth of positrons is shown on the upper horizontal axis. The $S$ value corresponding to the annihilation of positrons in defect-free GaN ($S_f$) was 0.442 [12–14]. For the as-implanted sample, the observed $S$ values were higher than $S_f$, indicating the trapping of positrons by vacancy-type defects. The $S$ values for the damaged region ($E$=1–15 keV) were increased by annealing after 1000°C, but they started to decrease above 1100°C annealing. For the samples annealed above 1300°C, the $S$ value was close to $S_f$, suggesting that the trapping of positrons by vacancies is almost negligible. The solid curves shown in Fig. 1 are fits to the experimental data. Figure 2 shows the derived depth distributions of $S$ and Mg. No significant change in the Mg profiles was observed up to 1300°C annealing. For the sample annealed at 1000°C, the increase in $S$ occurred below 700 nm, and this region agreed with the box profile of Mg, suggesting that the agglomeration of vacancy-type defects mainly occurred in the region with high [Mg].

The annealing behaviors of the $S$ values for Mg-implanted GaN with [Mg] of $1\times10^{17}$–$1\times10^{19}$ $cm^{-3}$ were reported by ref. 22. After annealing at 1300°C, the $S$ value increased as [Mg] decreased. This suggests that the primary origin of the decrease in $S$ is a partial activation of Mg by high-temperature annealing, resulting in a decrease of the Fermi level position. The downward shift of the Fermi level position causes a change in the charge state of vacancies from neutral to positive ($V^0 \rightarrow V^+$). The trapping rate of positrons for a positively charged vacancy is smaller than that for a neutral or negatively charged vacancy [9]. Thus, the observed decrease in the $S$ value for the annealed samples (Figs. 1 and 2) can be attributed to the downward shift of the Fermi level position by high-temperature annealing.

Figure 3 shows the annealing behavior of the $S$ value measured by the coincidence Doppler broadening technique at

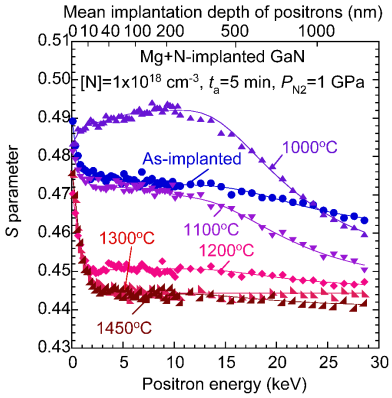


**Fig. 1.** $S$ parameters as function of incident positron energy $E$ for Mg-implanted GaN with sequential N-implantation before and after annealing at 1000–1450°C. Solid curves are fits to experimental data.

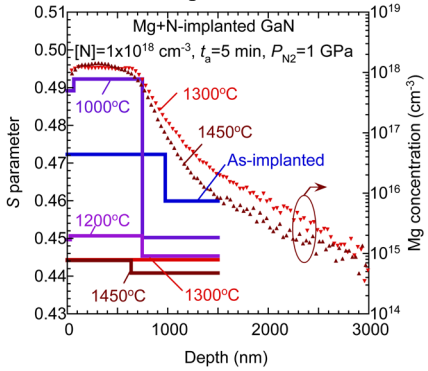


**Fig. 2.** Depth distributions of $S$ obtained from analysis of $S$–$E$ curves shown in Fig. 1 (solid lines) and those of Mg after annealing at 1300°C and 1450°C (triangles).

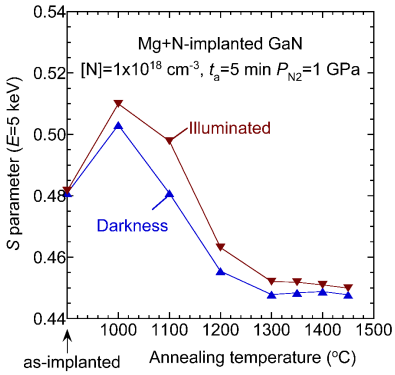


**Fig. 3.** $S$ parameter measured at $E$=5 keV as function of annealing temperature for Mg-implanted GaN with sequential N-implantation. Measurements were performed in darkness and under He-Cd illumination.

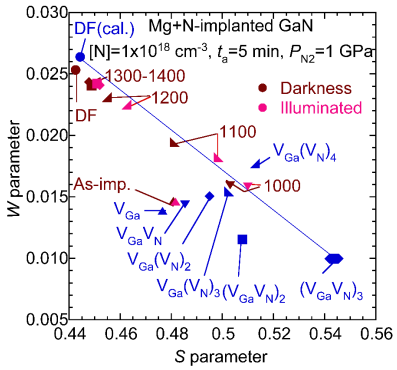


**Fig. 4.** *S*–*W* plots for Mg-implanted GaN with sequential N-implantation before (As-imp.) and after annealing (1000–1400°C. Measurements were done in darkness (brown symbols) and under He-Cd illumination (pink symbols). (*S*,*W*) value for defect-free GaN is shown as "DF." (*S*,*W*) values obtained by simulations for defect-free GaN [$D_{F(cal.)}$] and typical vacancy-type defects are shown as blue symbols.

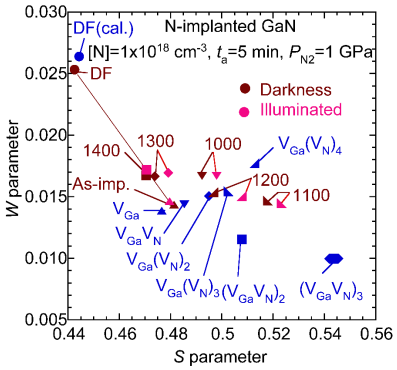


**Fig. 5.** *S*–*W* plots for N-implanted GaN measured in darkness and under He-Cd illumination.

*E*=5 keV ([N]=1×10$^{18}$ cm$^{-3}$ and $P_{N2}$=1 GPa) [15]. The spectra were also measured under the illumination of a He-Cd laser. The difference between the *S* values measured in darkness and under illumination can be attributed to the change in the charge state of vacancy-type defects from positive to neutral by the capturing of excited electrons by illumination ($V^+ + e^- \rightarrow V^0$) [12–14]. The illumination effect tended to decrease after annealing above 1200°C. This can be attributed to the suppression of electron capture by vacancies resulting from the activation of Mg by a higher annealing temperature.

Figures 4 and 5 show *S*–*W* relationships for the Mg-implanted GaN with sequential N-implantation and N-implanted GaN ([N]=1×10$^{18}$ cm$^{-3}$ and $P_{N2}$=1 GPa) calculated using the coincidence Doppler broadening spectra, respectively [15]. During the measurements, the value of *E* was fixed at *E*=5 keV. The (*S*,*W*) value corresponding to the positron annihilation in a defect-free GaN is shown as "DF" (defect-free). The (*S*,*W*) values measured in darkness and under illumination are shown as brown and pink symbols, respectively. The (*S*,*W*) value calculated from the simulated spectrum for the delocalized state is shown as "DF(cal.)." The simulated (*S*,*W*) values for typical vacancy-type defects are also shown in the figures (blue symbols).

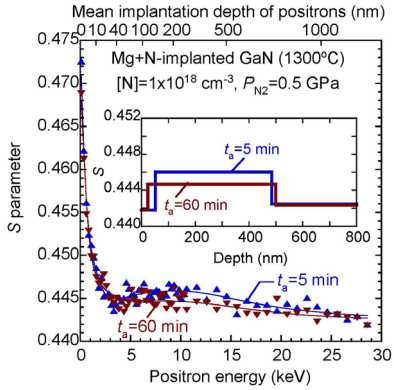


**Fig. 6.** *S*–*E* relationships for Mg-implanted GaN with sequential N-implantation. Annealing temperature was 1300°C, and annealing times (5 and 60 min) are shown in figure. Inset shows depth distributions of *S* obtained from analysis.

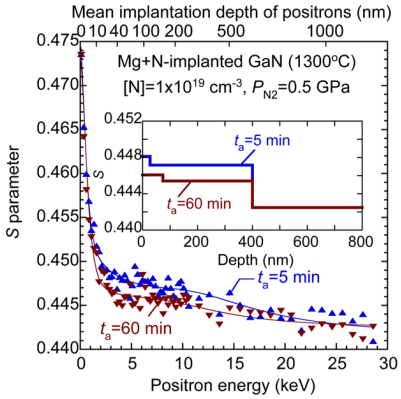


**Fig. 7.** *S*–*E* relationships for Mg-implanted GaN with sequential N-implantation. Inset shows depth distributions of *S* obtained from analysis.

For the as-implanted samples (As-imp.), the (*S*,*W*) values were close to the values for $V_{Ga}$ and $V_{Ga}V_N$. Thus, the major defect species can be identified as $V_{Ga}$-type defects. For the Mg-implanted GaN with sequential N-implantation (Fig. 4), the (*S*,*W*) values for the samples annealed above 1000°C were located along the line connecting the (*S*,*W*) values for defect-free GaN and $(V_{Ga}V_N)_3$, suggesting that the major defect species was vacancy clusters. Above 1100°C, the (*S*,*W*) value approached the defect-free value, which is attributed to the downward shift of the Fermi level position as discussed above.

For N-implanted GaN after annealing at 1000–1100°C (Fig. 5), the value shifted to the right-hand side, suggesting the agglomeration of vacancy-type defects. After 1200°C annealing, however, the (*S*,*W*) value shifted towards the left-hand side. From the observed annealing behavior of the (*S*,*W*) value, it can be concluded that the shrinkage of vacancy-type defects starts above 1200°C, and this can be attributed to recombinations between vacancy clusters and excess N atoms. The result also suggests that sequential N-implantation effectively suppresses the agglomeration of vacancies; however, the sample must be annealed above 1200°C to achieve this effect. In Figs. 4 and 5, the (*S*,*W*) values tended to show a right-hand shift under the illumination. The increase in

the number of $V_N$ coupled with $V_{Ga}$ caused the right-hand change in the *S*–*W* plot. Thus, the vacancy clusters acting as electron trapping centers are considered to have more $V_N$ than neutral or negatively charged clusters detected in darkness.

Figures 6 and 7 show the *S*–*E* relationships for Mg-implanted GaN with sequential N-implantation with different [N]s, ($1\times10^{18}$ and $1\times10^{19}$ $cm^{-3}$), respectively ($P_{N2}$=0.5 GPa, $t_a$=5 and 60 min). The depth distributions of *S* obtained from the analysis are shown in the insets in Figs. 6 and 7. The *S* value in the damaged region decreased as the annealing time increased. Figure 8 shows the annealing time dependence of the *S* value measured for Mg-implanted GaN with sequential N-implantation ([N]=$1\times10^{18}$, $3\times10^{18}$, and $1\times10^{19}$ $cm^{-3}$). These *S* values were calculated from coincidence Doppler broadening spectra measured at *E*=8 keV. For both measurements in darkness and under illumination, the *S* values for the sample with [N]=$3\times10^{18}$ $cm^{-3}$ were smaller than those for the samples with [N]=$1\times10^{18}$ and $1\times10^{19}$ $cm^{-3}$, suggesting that the residual vacancy concentration after annealing at 1300°C was low when the ratio of [N] to [Mg] was three.

Figure 9 shows PL spectra for Mg-implanted GaN with sequential N-implantation ([N]=$1\times10^{18}$, $3\times10^{18}$, and $1\times10^{19}$ $cm^{-3}$). The annealing temperature, annealing time, and $N_2$ pressure were 1300°C, 60 min, and 0.5 MPa, respectively. The sharp luminescence peak at 3.5 eV corresponds to the recombination of excitons bound to a $Mg_{Ga}$ acceptor (acceptor bound exciton: ABE), and the origin of a broad ultraviolet luminescence (UVL) band (2.6–3.4 eV) is a free electron or a shallow donor to a $Mg_{Ga}$ acceptor transition [23,24]. Thus, the increases in the intensities of the ABE peak and the UVL band relate to the increase in the concentration of $Mg_{Ga}$ and the decrease in the concentration of defects that act as NRCs. As shown in the inset of Fig. 9, the highest ABE peak intensity was obtained for the sample with [N]=$3\times10^{18}$ $cm^{-3}$, which can be associated with the observed suppression in the concentration of residual vacancies in this sample (Fig. 8).

For the sample with [N]=$1\times10^{18}$ $cm^{-3}$, a broad luminescence band at 2.1–2.6 eV was observed, but it was suppressed for the samples with [N]=$3\times10^{18}$ and $1\times10^{19}$ $cm^{-3}$. This green luminescence (GL) band is often observed for Mg-implanted GaN [24] and assigned to a transition involving $V_N$. Thus, the suppression of the GL band is due to the recombination of $V_N$ and N by sequential N-implantation. However, the total luminescence intensity decreased due to the introduction of NRCs for the sample with [N]=$1\times10^{19}$ $cm^{-3}$.

Figure 10 shows images of the (a) Mg-implanted GaN with sequential N-implantation and (c) N-implanted GaN after annealing at 1400°C obtained by LAADF-STEM [15]. Their magnified images are shown in (b) and (d), respectively. Bright dots were observed in the N-implanted sample. Their origin has been attributed to nano-scale intrinsic defects; an extra Ga atomic plane inserted between the Ga planes of the matrix [25,26]. For the Mg-implanted sample with N-implantation, both bright dots and circles were observed. The nature of the latter defects was identified as collapsed vacancy disks forming intrinsic dislocation loops [25,26]. Since the formation of such dislocation loops requires the removal of both Ga and N atoms from the inside of the loops, the $V_{Ga}$-rich condition for the N-implanted GaN can be the origin of the suppression of the formation of such secondary defects.

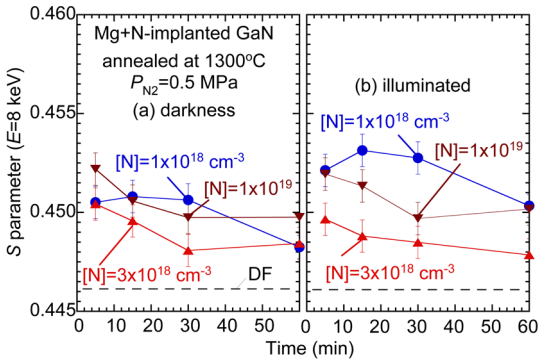


**Fig. 8.** *S* parameters as function of annealing time for Mg-implanted GaN with sequential N-implantation ([N]=$1\times10^{18}$, $3\times10^{18}$, and $1\times10^{19}$ $cm^{-3}$). Annealing temperature was 1300°C. Measurements were performed in (a) darkness and (b) under illumination.

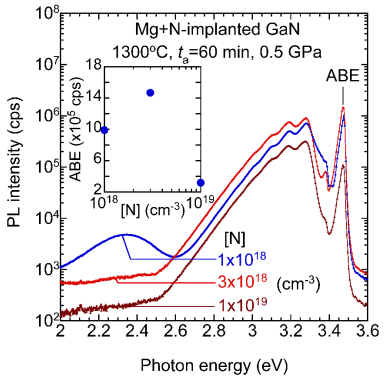


**Fig. 9.** PL spectra for Mg-implanted GaN with sequential N-implantation. Annealing temperature and annealing time were 1300°C and 60 min, respectively. Inset shows PL peak intensities corresponding to ABE as function of [N].

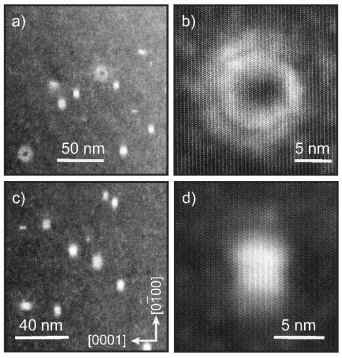


**Fig. 10.** LAADF-STEM images of (a) Mg-implanted GaN with sequential N-implantation, (c) N-implanted GaN ([N]=$1\times10^{18}$ $cm^{-3}$). Their magnified images are shown in (b) and (d), respectively. All samples were annealed at 1400°C ($t_a$= 5 min).

## IV. Conclusion

Annealing behaviors of vacancy-type defects in ion-implanted GaN were studied by positron annihilation. For as-implanted samples, the major defect species was identified as $V_{Ga}$-type defects. For N-implanted GaN, the size of the vacancies increased as the annealing temperature increased up to 1100°C and then shrank above 1200°C. This behavior was attributed to recombinations between $V_N$-type defects and implanted N atoms. For Mg-implanted GaN with sequential N-implantation, the major defect species after annealing above 1000°C was vacancy clusters such as $(V_{Ga}V_N)_3$. Positively charged vacancy clusters were formed after annealing above 1000°C, and they had more $V_N$ than neutral or negatively charged clusters. The effect of sequential N-implantation was most effective when the ratio of [N] to [Mg] was three. After annealing at 1400°C, the major secondary defects were nano-scale intrinsic defects and collapsed vacancy disks forming intrinsic dislocation loops, and the formation of the latter defects was suppressed in sequential N-implantation.

## References


[1] B. J. Baliga, "Power semiconductor device figure of merit for high-frequency applications," *Electron Device Lett.*, vol. 10, no. 10, Oct. 1989, pp. 455–457, doi: 10.1109/55.43098.

[2] Y. Zhang, A. Dadger, and T. Palacios, "Gallium nitride vertical power devices on foreign substrates: a review and outlook," J. Phys. D: Appl. Phys, vol. 51, June 2018, Art no. 273001, doi: 10.1088/1361-6463/aac8aa.

[3] L. H. Hsu, Y. Y. Lai, P. T. Tu, C. Langpoklakpam, Y. T. Chang, Y. W. Huang, W. C. Lee, A. J. Tzou, Y. J. Cheng, C. H. Lin, H. C. Kuo, and E. Y. Chang, "Development of GaN HEMTs fabricated on silicon, silicon-on-insulator, and engineered substrates and the heterogeneous integration," Micromachines, vol. 12, Sept. 2021, Art. no 1159, doi: 10.3390/mi12101159.

[4] T. Kachi, T. Narita, H. Sakurai, M. Matys, K. Kataoka, K. Hirukawa, K. Sumida, M. Horita, N. Ikarashi, K. Sierakowski, M. Bockowski, and J. Suda, "Process engineering of GaN power devices via selective-are p-type doping with ion implantation and ultra-high-pressure annealing," J. Appl. Phys., vol. 132, Oct. 2022, Art. no. 130901, doi: 10.1063/5.0107921.

[5] H. Sakurai, M. Omori, S. Yamada, Y. Furukawa, H. Suzuki, T. Narita, K. Kataoka, M. Horita, M. Bockowski, J. Suda, and T. Kachi, "Highly effective activation of Mg-implanted p-type GaN by ultra-high-pressure annealing," Appl. Phys. Lett., vol. 115, Sept. 2019, Art. no. 142104, doi: 10.1063/1.5116866.

[6] K. Sierakowski, R. Jakiela, B. Lucznik, P. Kwiatkowski, M. Iwinska, M. Turek, H. Sakurai, T. Kachi, and M. Bockowski, "High Pressure Processing of Ion Implanted GaN," Electronics, vol. 9, Aug. 2020, Art. no. 1380, doi: 10.3390/electronics9091380.

[7] J. L. Lyons and C. G. Van de Walle, "Computationally predicted energies and properties of defects in GaN," Npj Comput. Mat., vol. 3, March 2017, Art. no. 12, doi: 10.1038/s41524-017-0014-2.

[8] R. Tanaka, S. Takashima, K. Ueno, H. Matsuyama, and M. Edo, "Demonstration of 1200 V/1.4 mΩ cm2 vertical GaN planar MOSFET fabricated by an all ion implantation process," Jpn. J. Appl. Phys., vol. 59, April 2020, SGGD02, doi: 10.7567/1347-4065/ab6347.

[9] R. Krause-Rehberg, H. S. Leipner, Positron Annihilation in Semiconductors, Solid-State Sciences vol. 127, Springer-Verlag, Berlin, 1999.

[10] F. Tuomisto and I. Makkonen, "Defect identification in semiconductors with positron annihilation: Experiment and theory," Rev. Mod. Phys., vol. 85, Nov. 2013, Art. no. 1583, doi: 10.1103/RevModPhys.85.1583

[11] K. Saarinen, T. Laine, S. Kuisma, J. Nissila, P. Hautojarvi, L. Dobrzynski, J. M. Baranowski, K. Pakula, R. Stepniewski, M. Wojdak, A. Wysmolek, T. Suski, M. Leszczynski, I. Grzegory, S. Porowski, "Observation of Native Ga Vacancies in GaN by Positron Annihilation," Phys. Rev. Lett., vol. 79, Oct. 1997, Art. no. 3030, doi: 10.1103/PhysRevLett.79.3030.

[12] A. Uedono, H. Iguchi, T. Narita, K. Kataoka, W. Egger, T. Koschine, C. Hugenschmidt, M. Dickmann, K. Shima, K. Kojima, S. F. Chichibu, and S. Ishibashi. "Annealing behavior of vacancy-type defects in Mg- and H-implanted GaN studied using monoenergetic positron beams," Phys. Stat. Sol. B, vol. 256, no. 10, May 2019, Art. no. 1900104, doi: 10.1002/pssb.201900104.

[13] A. Uedono, R. Tanaka, S. Takashima, K. Ueno, M. Edo, K. Shima, K. Kojima, S.F. Chichibu, S. Ishibashi, "Dopant activation process in Mg-implanted GaN studied by monoenergetic positron beam," Sci. Rep., vol. 11, no. 1, Oct. 2021, Art. no. 20660, doi: 10.1038/s41598-021-00102-2.

[14] A. Uedono, A., H. Sakurai, J. Uzuhashi, T. Narita, K. Sierakowski, S. Ishibashi, S. F. Chichibu, M. Bockowski, J. Suda, T. Ohkubo, N. Ikarashi, K. Hono, and T. Kachi, "Effect of ultra-high-pressure annealing on defect reactions in ion-implanted GaN studied by positron annihilation," Phys. Stat. Sol. B, vol. 259, May 2022, Art. no. 2200183, doi: 10.1002/pssb.202200183.

[15] A. Uedono, R. Tanaka, S. Takashima, K. Ueno, M. Edo, K. Shima, S. F. Chichibu, J. Uzuhashi, T. Ohkubo, S. Ishibashi, K. Sierakowski, and M. Bockowski, "Characterization of vacancy-type defects in Mg- and N-implanted GaN by using a monoenergetic positron beam," in Proc. Int. Workshop on Junction Technology (IWJT), 2025.

[16] J. Uzuhashi and T. Ohkubo, "Systematic study of FIB-induced damage for the high-quality TEM sample preparation," Ultramicroscopy, vol. 262, April 2024, Art. no. 113980, doi: 10.1016/j.ultramic.2024.113980.

[17] J. Uzuhashi, Y. Yao, T. Ohkubo, and T. Sekiguchi, "Experimental investigation and simulation of SEM image intensity behaviors for developing thickness-controlled S/TEM lamella preparation via FIB-SEM," Microscopy, vol. 74, no. 4, January 2025, pp. 279-285, doi: 10.1093/jmicro/dfaf006.

[18] A. Van Veen, H. Schut, M. Clement, J. M. M. de Nijs, A. Kruseman, and M. R. IJpma, "VEPFIT applied to depth profiling problems," Appl. Surf. Sci., vol 85, no. 2, Jan. 1995, pp. 216–224.

[19] S. Ishibashi, T. Tamura, S. Tanaka, M. Kohyama, and K. Terakura, "Ab initio calculations of electric-field-induced stress profiles for diamond/c-BN (110) superlattices," Phys. Rev. B, vol. 76, Oct. 2007, Art. no. 153310, doi: 10.1103/PhysRevB.76.153310.

[20] P. E. Blochl, "Projector augmented-wave method," Phys. Rev. B, vol. 50, Dec. 1994, Art. no. 17953, doi: 10.1103/PhysRevB.50.17953.

[21] S. Ishibashi, A. Uedono, H. Kino, T. Miyake, and K. Terakura, "Computational study of positron annihilation parameters for cation monovacancies and vacancy complexes in nitride semiconductor alloys," J. Phys. Cond. Matt., vol. 31, Aug. 2019, Art. no. 475401, doi: /10.1088/1361-648X/ab35a4.

[22] A. Uedono, S. Takashima, M. Edo, K. Ueno, H. Matsuyama, W. Egger, T. Koschine, C. Hugenschmidt, M. Dickmann, K. Kojima, S. F. Chichibu, and S. Ishibashi, "Carrier trapping by vacancy-type defects in Mg-implanted GaN studied using monoenergetic positron beams," Phys. Stat. Sol. B, vol. 255, Dec. 2017, Art. no. 1700521, doi: 10.1002/pssb.201700521.

[23] M. A. Reshchikov and H. Morkoc, "Luminescence properties of defects in GaN," J. Appl. Phys., vol. 97, March 2005, Art. No. 061301, doi: 10.1063/1.1868059.

[24] K. Shima, H. Iguchi, T. Narita, K. Kataoka, K. Kojima, A. Uedono, and S. F. Chichibu, "Shima, K., H. Iguchi, T. Narita, K. Kataoka, K. Kojima, A. Uedono, and S. F. Chichibu, "Room-temperature photoluminescence lifetime for the near-band-edge emission of $(000\bar{1})$ p-type GaN fabricated by sequential ion-implantation of Mg and H," Appl. Phys. Lett., vol. 113, Nov. 2018, Art. no. 191901, doi: 10.1063/1.5041879.

[25] K. Iwata, H. Sakurai, S. Arai, T. Nakashima, T. Narita, K. Kataoka, M. Bockowski, M. Nagao, J. Suda, T. Kachi, and N. Ikarashi, "Defect evolution in Mg ions implanted GaN upon high temperature and ultrahigh N2 partial pressure annealing: Transmission electron microscopy analysis," J. Appl. Phys., vol. 127, March 2020, Art. no. 105106, doi: 10.1063/1.5140410.

[26] E. Kano, K. Kataoka, J. Uzuhashi, K. Chokawa, H. Sakurai, A. Uedono, T. Narita, K. Sierakowski, M. Bockowski, R. Otsuki, K. Kobayashi, Y. Itoh, M. Nagao, T. Ohkubo, K. Hono, J. Suda, T. Kachi, N. Ikarashi, "Atomic resolution analysis of extended defects and Mg agglomeration in Mg-ion-implanted GaN and their impacts on acceptor formation," J. Appl. Phys., vol. 132, Aug. 2022, Art. no. 065703, doi: 10.1063/5.0097866.